CHIN. PHYS. LETT. Vol. 35, No. 8 (2018) 084501

Dynamics of a Rotating Sphere on Free Surface of Vibrated Granular Materials *

Adones B. Dengal[1,2], Joel T. Maquiling[1**]

[1] *Geophysics Research Laboratory, Department of Physics, School of Science and Engineering, Ateneo de Manila University, Quezon 1108, Philippines*

[2] *Department of Physics, College of Natural Sciences and Mathematics, Mindanao State University, Marawi 9700, Philippines*

(Received 11 April 2018)

We investigate the rotational dynamics of a low-density sphere on the free surface of a vertically vibrated granular material (VGM). The dynamical behavior of the sphere is influenced by the external energy input from an electromagnetic shaker which is proportional to ε, where ε is equal to the ratio between the square of the dimensionless acceleration Γ and the square of the vibration frequency f of the container. Empirical results reveal that as the VGM transits from local-to-global convection, an increase in ε generally corresponds to an increase in the magnitudes of the rotational $\omega_{\rm RS}$ and translational $v_{\rm CM}$ velocities of the sphere, an increase in the observed tilting angle $\theta_{\rm bed}$ of the VGM bed, and a decrease in the time $t_{\rm wall}$ it takes the sphere to roll down the tilted VGM bed and hit the container wall. During unstable convection, an increase in ε results in a sharp decrease in the sphere's peak and mean $\omega_{\rm RS}$, and a slight increase in $t_{\rm wall}$. For the range of ε values covered in this study, the sphere may execute persistent rotation, wobbling or jamming, depending on the vibration parameters and the resulting convective flow in the system.

PACS: 45.70.−n, 45.70.Mg, 47.55.Lm, 45.50.−j DOI: 10.1088/0256-307X/35/8/084501

Vibrated granular materials exhibit a wide range of complex fluid-like behavior that deviates from conventional theories of fluid dynamics.[1−3] Depending on the sizes and shapes of the constituent particles,[4] the number of particle layers,[5] the geometry of the system,[6] and the vibration parameter settings (i.e., f and $\Gamma = a/g$, where a is the peak acceleration of the container, and g is the acceleration due to gravity), a vertically vibrated granular system may transition across different motion states such as bouncing bed, undulation, granular Leidenfrost effect, local or global convection, and granular gas.[7−10] Fundamental research on the complex behaviors of VGMs has gained momentum in recent decades due to their importance in various industrial processes such as drying, powder mixing or segregation, and vibratory finishing,[2,6,11] as well as in the understanding and mitigation of geophysical processes such as earthquakes, avalanches, landslides, and debris flow.[12]

The interaction between a VGM and an elastic or inelastic object is another complex issue that has sparked widespread interest among scientists and engineers. A ball placed on the bare surface of a vertically vibrated plate can exhibit chaotic dynamics, i.e., it can bounce persistently by way of periodic motion, period-doubling cascade, and chaos.[13] However, when the same ball is placed on the surface of the VGM instead, 'non-bouncing' scenarios can be observed. For instance, the ball can stay afloat on the free surface of the granular bed, or sink to the bottom of the container, or remain suspended in the middle of the VGM.[14]

In the series of experiments and computer simulations of Zamankhan,[6,11] a large but low-density plastic spherical intruder (initially placed onto the free surface of the VGM) may undergo sinking and recirculation subject to f and Γ, the material properties of the granular particles, geometry of the container, and air pressure inside the container. For instance, the intruder will stay afloat when the VGM consists of 1500-μm and of 500-μm glass beads. In both the cases, the granular convections are not strong enough to drag the intruder into the bed. When 200-μm glass beads are used instead, the intruder sinks to the bottom of both the tulip-shaped and the straight conical perspex containers due to vigorous granular convection, i.e., when $\Gamma > 6$ at 49 Hz and 1 atm. Yet, the intruder is able to recirculate to the free surface of the granular bed only in the tulip-shaped container, not in the latter. Furthermore, even under the same VGM conditions, the intruder always stays afloat when the air pressure inside the container decreases far below 1 Torr.

Although the complex behavior of an intruder in vibrated granular systems has been extensively studied previously, to the best of our knowledge, most (if not all) of the experiments, mathematical models, and numerical simulations published so far have focused on the sinking and rising processes.[14−18] The present work focuses on the dynamics of a sphere that does not just stay afloat but exhibits persistent rotation on the free surface of the VGM undergoing convection. Specifically, this study examines the effect of varying f and Γ on the translational speed $v_{\rm CM}$ of the sphere's

*Supported by the CHED-FDP Ⅱ Program of the Commission on Higher Education of the Philippines.

**Corresponding author. Email: jmaquiling@ateneo.edu

© 2018 Chinese Physical Society and IOP Publishing Ltd

center of mass and the rotational speed $\omega_{\rm RS}$ of the sphere about its center of mass.

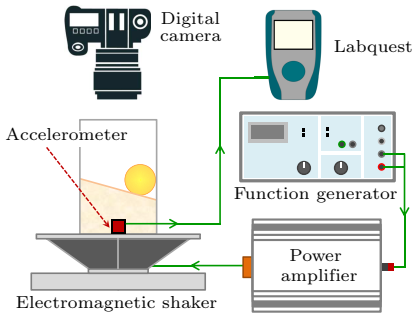

Fig. 1. The experimental setup consists of a cylindrical plexiglas container (inner diameter $d_{\rm c} = 9.4\,{\rm cm}$, inner height $H_{\rm c} = 14.2\,{\rm cm}$) that is fixed onto an electromagnetic shaker. The shaker is vertically driven by sinusoidal signals from a digital function generator (Pasco Scientific, PI-9587C) and a power amplifier. The vibration acceleration a is measured through a z-axis accelerometer (Vernier) mounted on the shaker and connected to a standalone interface (LabQuest).

A thin spherical shell (Ping-Pong ball) of mass $m_{\rm s} = 2.0\,{\rm g}$ and outer diameter $d_{\rm s} = 3.95\,{\rm cm}$ is placed onto the free surface of the granular bed made up of smooth spherical soda glass beads with mean diameter $d_{\rm g} = 2.9 \pm 0.5\,{\rm mm}$, density $\rho_{\rm g} = 2.4\,{\rm g/cm^3}$, and total mass $m_{\rm g} = 500\,{\rm g}$. The static packing height of the granular bed in the cylindrical container is $H_{\rm g} = 4.7 \pm 0.1\,{\rm cm}$. Eight sets of vibration parameter combinations are employed (Table 1), and four independent runs are conducted per vibration setting. In each run, the granular system is initialized and then vibrated for over 3 min. The top-view motion of the sphere is recorded using a Fujifilm XT-10 digital camera fixed on a tripod. The slope $\theta_{\rm bed}$ of the free surface of the granular bed is measured using an Arduino-based MPU-6050 sensor after every run.

Table 1. Vibration parameter settings.

f (Hz)	a (m/s^2)	Γ	A (mm)	$(\Gamma^2/f^2)\,(10^{-2}\,{\rm s}^2)$	$\theta_{\rm bed}$ (deg)
20	61.14±0.93	6.23	3.87	9.71: ε_8	1.94±0.26
25	52.27±0.69	5.33	2.12	4.54: ε_7	7.45±0.88
30	44.21±0.69	4.51	1.24	2.26: ε_6	9.10±1.05
35	41.28±0.56	4.21	0.85	1.45: ε_5	10.51±0.71
40	35.00±0.62	3.57	0.55	0.80: ε_4	9.53±0.75
45	30.15±1.16	3.07	0.38	0.47: ε_3	8.08±1.09
50	28.47±0.77	2.90	0.29	0.34: ε_2	7.69±1.32
55	26.35±0.74	2.69	0.22	0.24: ε_1	5.34±1.23

From the measured a values, the corresponding Γ values are calculated using the relationship $\Gamma = a/g$. Moreover, since $a = A\omega^2$, where A is the physical vibration amplitude of the container and $\omega = 2\pi f$, then $A = a/(4\pi^2 f^2)$. In Table 1, only the standard deviations (denoted by the ± sign) of the measured parameters are included. From the raw videos recorded at 60 frames per second, image snapshots are automatically extracted every 0.25-s time interval using Freestudio v.5.0.6. Only the first 200 s or the first $N = 801$ snapshots of every video are retained for image processing and further analyses.

To track the two-dimensional (top-view) translation of the sphere's center of mass on the surface of the VGM, the snapshots are imported as an image sequence in ImageJ and the corresponding centroid positions $c_{x,i}$ and $c_{y,i}$ of the sphere in frame i are determined for all frames in the sequence, i.e., for $i = 1, 2, \ldots, N$. The displacement $D_{{\rm CM},i}$ of the sphere's center of mass relative to its position in the previous frame $(i-1)$ is

$$D_{{\rm CM},i} = \sqrt{(c_x - c_{x,i-1})^2 + (c_y - c_{y,i-1})^2}, \quad (1)$$

for $i = 1, 2, \ldots, N$. For all the image sequences, the first frame is the initial frame, so $D_{\rm CM,1}$ is always equal to zero. From the displacement $D_{\rm CM} = \{D_{\rm CM,1}, D_{\rm CM,2}, \ldots, D_{\rm CM,N}\}$ in Eq. (1), the translational velocity $v_{\rm CM} = \{v_{\rm CM,1}, v_{\rm CM,2}, \ldots, v_{\rm CM,N}\}$ of the sphere's center of mass is simply $v_{{\rm CM},i} = D_{{\rm CM},i}/\Delta t$ $(i = 1, 2, \ldots, N)$, where $\Delta t = 0.25\,{\rm s}$. Also, $t_{\rm wall}$ is manually determined by scanning the image sequence chronologically to see at which frame i the moving sphere reaches the container wall, i.e., $t_{\rm wall} = (i-1)\Delta t$.

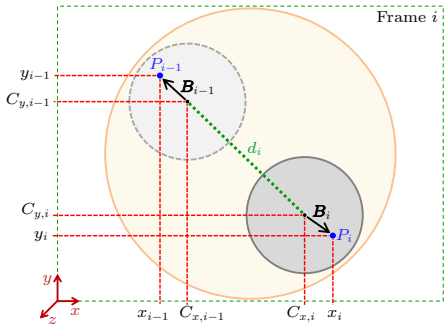

Fig. 2. Illustration of the parameters measured via image processing.

To track the rotational motion of the sphere, marker grids on the sphere's surface are used. For a particular image sequence, a target point P is chosen such that P is present in two consecutive frames (see P_{i-1} and P_i in Fig. 2). When two or more marker points are available, the point with the largest angular displacement in the two frames stated above is chosen. The frame-to-frame angular displacement Φ_i can be determined using two vectors $\boldsymbol{B}_{i-1}$ and $\boldsymbol{B}_i$ (Fig. 2), which represent the same vector $\boldsymbol{B}$ but rotated at an angle Φ_i about a certain instantaneous axis of rotation. From the definition of the dot product, $\boldsymbol{B}_{i-1} \cdot \boldsymbol{B}_i = |\boldsymbol{B}_{i-1}||\boldsymbol{B}_i| \cos\Phi_i$. Thus

$$\Phi_i = \cos^{-1}\left(\frac{B_{x,i-1}B_{x,i} + B_{y,i-1}B_{y,i} + B_{z,i-1}B_{z,i}}{|\boldsymbol{B}_{i-1}||\boldsymbol{B}_i|}\right). \quad (2)$$

The magnitudes $|\boldsymbol{B}_{i-1}|$ and $|\boldsymbol{B}_i|$ are both equal to the radius $r_{\rm s} = 1.975\,{\rm cm}$ of the sphere because vectors $\boldsymbol{B}_{i-1}$ and $\boldsymbol{B}_i$ both originate at the centroid of

the sphere and terminate on the surface. The 3D vector components in Eq. (2) are derived using spherical geometry.

Based on Xie *et al.*,[19] the average incoming power P_{ave} of a vibrated granular system can be expressed as

$$P_{\text{ave}} = \frac{(m_{\text{g}} + m_{\text{s}})A^2\omega^2}{4} = \frac{(m_{\text{g}} + m_{\text{s}})g^2}{16\pi^2}\frac{\Gamma^2}{f^2}, \quad (3)$$

which suggests that the energy gain of a vibrated granular system is proportional to $A^2(2\pi f)^2$ or equivalently, to the ratio Γ^2/f^2. In a subsequent study, Xie *et al.*[15] described the activation extent of small particle convection using a unified parameter $y = (\Gamma^2/f^2)p$, where p is the air pressure inside the container at equilibrium state. Following Xie *et al.*,[15,19] the present work investigates the dynamical behavior of the sphere with respect to the ratio $\varepsilon = \Gamma^2/f^2$, with p being constant at 1 atm. Empirical trends in the behaviors of θ_{bed}, peak ω_{RS}, mean ω_{RS}, peak v_{CM}, and mean v_{CM} as a function of ε are presented in Fig. 3. For the range of ε values covered in this study, the dynamics of the system can be classified into four zones. Table 2 summarizes the characteristic trends for each of the four zones (I, Ⅱ, Ⅲ, and Ⅳ) accordingly.

Under different combinations of f and Γ and their corresponding ε, the VGM exhibits diverse geometrical formations and convection modes, which influence the motion of the sphere on the free surface of the granular bed. For example, when the energy input is considerably low ($\varepsilon_1 = 0.0024\,\text{s}^2$), θ_{bed} is minimal ($\theta_1 \approx 5.34°$) and the VGM shows local convection only. In this case ($\Gamma = 2.69$ at $f = 55$ Hz), Γ is not large enough for the convective flow to penetrate the entire bed. As a result, the sphere only exhibits minimal rotational and translational motion on the surface of the VGM, with mean ω_{RS} of 0.203 ± 0.170 rad/s and mean v_{CM} of 0.485 ± 0.016 mm/s.

As the external energy input is increased by decreasing f or increasing A, the convective flow spreads from the surface layers to the bottom of the VGM until global convection occurs. For zone I, an increase in ε corresponds to an increase in all measured parameters (θ_{bed}, ω_{RS}, v_{CM}), but this is not true for zones Ⅱ–Ⅳ. In particular, there is an inflection point in the relationship between θ_{bed} and ε such that within zone Ⅱ, θ_{bed} increases with increasing ε until it reaches its maximum value ($\theta_4 \approx 10.51°$), and then it starts decreasing with increasing ε in zones Ⅲ and Ⅳ.

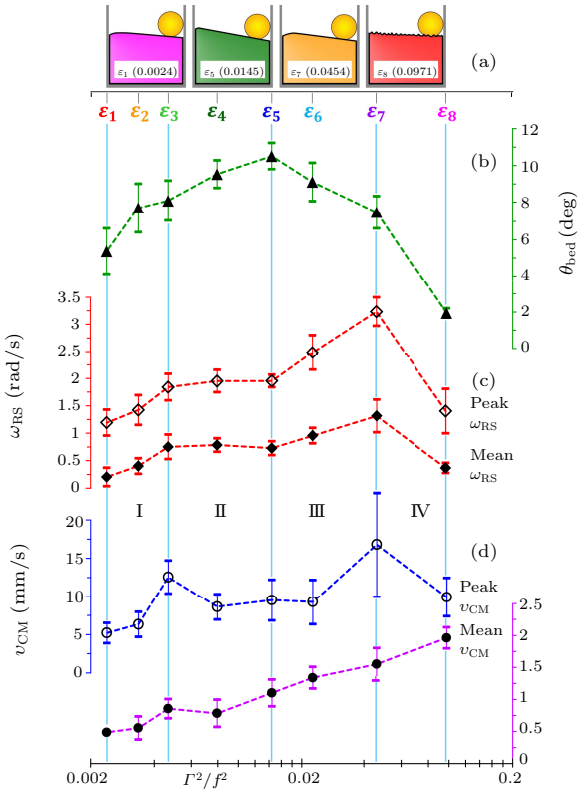

Fig. 3. (a) Schematic diagram of observed geometrical formations; and superimposed plots of (b) θ_{bed} versus ε, (c) peak ω_{RS} and mean ω_{RS} versus ε, and (d) peak v_{CM} and mean v_{CM} versus ε. Error bars represent the standard deviations of the measurements across different experimental runs.

Table 2. Behavior of the VGM-sphere system under different ε.

Zone	$\varepsilon\,(10^{-2}\text{s}^2)$	Characteristic behavior
Ⅰ	$0.24 \leqslant \varepsilon < 0.47$	θ_{bed} increases peak ω_{RS} and mean ω_{RS} increase peak v_{CM} and mean v_{CM} increase
Ⅱ	$0.47 \leqslant \varepsilon < 1.45$	θ_{bed} increases peak ω_{RS} and mean $\omega_{\text{RS}} \approx$ constant peak v_{CM} decreases, mean v_{CM} increases
Ⅲ	$1.45 \leqslant \varepsilon < 4.54$	θ_{bed} decreases peak ω_{RS} and mean ω_{RS} increase peak v_{CM} and mean v_{CM} increase
Ⅳ	$4.54 < \varepsilon \leqslant 9.71$	θ_{bed} decreases peak ω_{RS} and mean ω_{RS} decrease peak v_{CM} decreases, mean v_{CM} increases

The peak ω_{RS} and mean ω_{RS} exhibit identical trends all throughout the four zones. In zone Ⅱ, the mean ω_{RS} ranges only from 0.727 to 0.784 rad/s while the peak ω_{RS} is from 1.841 to 1.953 rad/s. Interestingly, both the parameters exhibit very minimal changes in zone Ⅱ despite the increase in both ε and

$\theta_{\rm bed}$. This can be attributed to two competing motion states of the sphere in this zone: persistent rotation; and active jamming, which is labelled (J) in the representative time series shown in Fig. 4(a). In zone Ⅲ, both peak $\omega_{\rm RS}$ and mean $\omega_{\rm RS}$ increase proportionally with ε until they reach their maximum values: 3.232±0.262 rad/s and 1.314±0.298 rad/s, respectively. In this zone, the sphere executes persistent rotation on the surface of the VGM, with low probability of jamming. When the input energy is increased further in zone Ⅳ, the VGM vibrates more vigorously and the slope of the bed flattens out, resulting in the decrease in both mean $\omega_{\rm RS}$ and peak $\omega_{\rm RS}$. When ε is considerably high ($\varepsilon_8 = 0.0971\,{\rm s}^2$ at 20 Hz), the VGM undergoes unstable convection similar to that reported by Zhang *et al.*[7] for high Γ and low f. Under these vibration conditions, the sphere's motion is primarily governed by wobbling instead of persistent rotation.

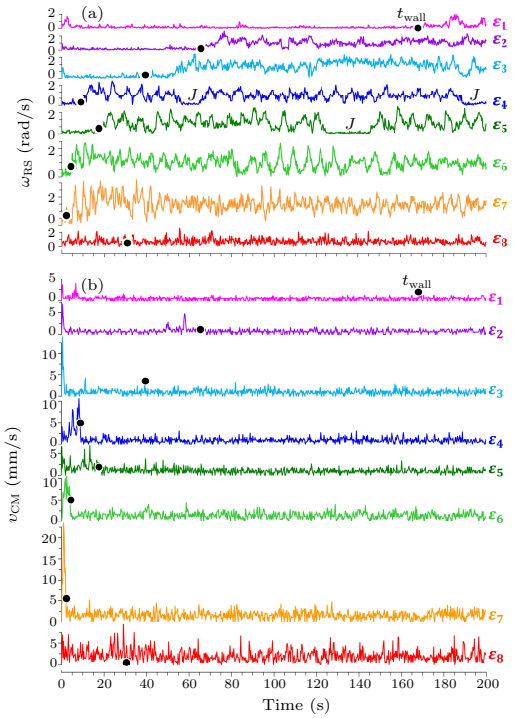

Fig. 4. Representative time series for (a) $\omega_{\rm RS}$ and (b) $v_{\rm CM}$. The black dots denote the location of the $t_{\rm wall}$.

In previous studies, the degree of fluidization of VGM has been reported to increase when the input energy is increased (by increasing Γ or A, or by decreasing f). As ε increases, the kinetic energy of the fluidized bed also increases, triggering an increase in the average velocity of the granular particles.[5,8,13,14,19] Additionally, the individual motion of the particles appears more erratic at large ε.[20] Such behavior of granular particles is the same behavior observed in the mean $v_{\rm CM}$ of the sphere. In fact, of the five parameters plotted in Fig. 3, only the mean $v_{\rm CM}$ shows direct proportionality to Γ^2/f^2 across all zones. By visual inspection of Fig. 4(b), it is also quite apparent that the fluctuations in the translational motion of the sphere become increasingly erratic at large ε. Figure 5 quantifies the fluctuations in $\omega_{\rm RS}$ and $v_{\rm CM}$ by plotting the velocity squared dispersions σ_ω^2 and $\sigma_{\rm v}^2$ against ε. In general, there is a positive trend in both σ_ω^2 versus ε, and $\sigma_{\rm v}^2$ versus ε as the VGM transits from local convection to global convection (i.e., from zones I to Ⅲ). A deviation from this trend is observed in zone Ⅳ where unstable convection occurs, i.e., when the sphere does not rotate persistently but wobbles around the VGM in roughly random directions, but with minimal angular displacements.

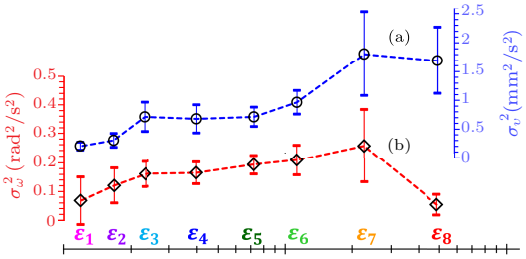

Fig. 5. Velocity squared dispersions σ_ω^2 and $\sigma_{\rm v}^2$ as a function of ε. Error bars represent the standard deviations of σ_ω^2 and $\sigma_{\rm v}^2$ across different runs.

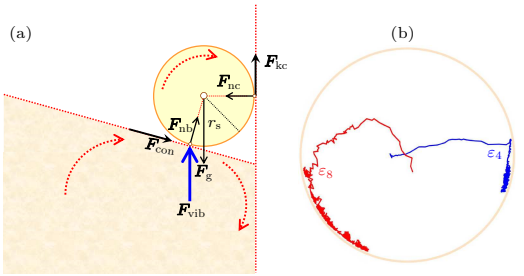

Fig. 6. (a) Free-body diagram of the sphere on the tilted bed, and (b) sample two-dimensional (x–y) track of the sphere's center of mass.

Figure 6(a) shows the forces acting on the rotating sphere and its general direction of rotation, as well as the direction of the convective flow of the VGM. The forces include the gravitational force $F_{\rm g}$, the normal force $F_{\rm nc}$ exerted by the container wall, the friction force $F_{\rm kc}$ between the rotating sphere and the wall, the normal force $F_{\rm nb}$ exerted by the tilted granular bed at the point of contact, the force $F_{\rm con}$ due to bead-sphere frictions and collisions, and the force $F_{\rm vib}$ due to the vertical vibration of the container. Of these forces, only $F_{\rm con}$, $F_{\rm kc}$, and $F_{\rm vib}$ contribute to the total torque acting on the sphere with respect to the rotation axis, which in this case is directed clockwise (into the page). The total clockwise torque on the sphere is

$$\tau_{\rm cw} = r_{\rm s}(F_{\rm vib}\sin\theta_{\rm bed} - F_{\rm con} - F_{\rm kc}). \qquad (4)$$

As exemplified in the representative time series for ε_4 and ε_5 depicted in Fig. 4(a), the sphere may get jammed even after having rotated persistently for a while. For jamming to occur, $\tau_{\rm CW}$ must be approximately zero. This condition is possible due to

the complex nonlinear behavior of the VGM, particularly in convection where there is high fluidization of particles.[7,8] The kinetic energy of the VGM is dissipated by friction and collisions,[14,19] which include bead-bead, bead-wall, bead-sphere, and sphere-wall frictions and collisions. Thus while the system appears to achieve dynamic equilibrium after the slope reaches $\theta_{\rm bed}$, the convective flow actually triggers the small particles to continuously rearrange themselves, causing $\theta_{\rm bed}$ to slightly fluctuate and the VGM system to move very slowly around the cylinder, as is evident in the sample tracks in Fig. 6(b). In essence, all the variables in Eq. (4) fluctuate to some extent, which may sometimes give rise to the jamming condition $\tau_{\rm CW} \approx 0$.

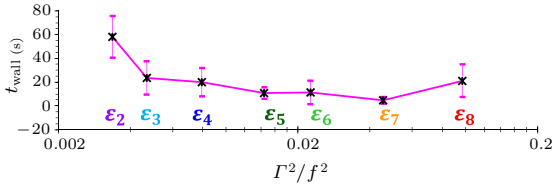

Fig. 7. Plot of $t_{\rm wall}$ as a function of ε. Error bars represent the standard deviations of $t_{\rm wall}$ across different runs.

In vibrated systems, the driving force governs the behavior of the system.[14] Naturally, $t_{\rm wall}$ is also influenced by the driving force as well as the convective motions of the small particles. For the range of ε values examined, $t_{\rm wall}$ is longest at ε_1 (103.2±66.5 s) when the input energy is lowest, and shortest at ε_7 (4.7±2.7 s) where $\omega_{\rm RS}$ is maximum. Figure 7 plots the behavior of $t_{\rm wall}$ as a function of ε from ε_2 to ε_8. In general, $t_{\rm wall}$ decreases with increasing ε across zones I–Ⅲ when the granular system transits from local-to-global convection. A minor increase in $t_{\rm wall}$ is observed when the increase in ε causes the convective flow to be unstable.

In summary, for the range of vibration parameter settings examined in this study (f: 20–55 Hz; Γ: 2.69–6.23; ε: 0.0024–0.0971), clear convective motion can be seen throughout the VGM. Upon initiation of the vertical vibration, both the glass beads and the sphere (which is initially placed at the center of the bed) acquire kinetic energy and begin to move. After considerable time, the geometrical formation stabilizes at an angle $\theta_{\rm bed}$, causing the sphere to roll down the tilted bed until it hits the container wall. The sphere then starts to rotate either persistently or intermittently, depending on the slope of the bed and the combination of vibration parameters.

As the VGM undergoes local-to-global convection, an increase in input energy Γ^2/f^2 generally results in an increase in both $\omega_{\rm RS}$ and $v_{\rm CM}$, and a decrease in $t_{\rm wall}$. During unstable convection, an increase in Γ^2/f^2 results in a sharp decrease in the sphere's peak $\omega_{\rm RS}$ and mean $\omega_{\rm RS}$, and a slight increase in $t_{\rm wall}$. Experimentally, the highest tilting angle of 10.51°±0.71° is observed at 35 Hz ($\Gamma = 4.21$), while the maximum rotation of the sphere is seen at 25 Hz ($\Gamma = 5.33$), signifying that a highly tilted granular bed does not automatically ensure the fastest rotation. Rather, to maximize the sphere's rotation on the free surface of the VGM, there must be an optimal combination of vibration parameters f, Γ, and A such that the energy gain of the VGM is at its highest possible value just below the unstable convection zone.

References

[1] Jaeger H, Nagel S and Behringer R 1996 *Rev. Mod. Phys.* **68** 1259
[2] Kruelle C A 2009 *Rev. Adv. Mater. Sci.* **20** 113
[3] Kakalios J 2005 *Am. J. Phys.* **73** 8
[4] Jain A, Metzger M J and Glasser B J 2013 *Powder Technol.* **237** 543
[5] Eshuis P, van der Weele K, van der Meer D et al 2007 *Phys. Fluids* **19** 123301
[6] Zamankhan P 2013 *Adv. Powder Technol.* **24** 1070
[7] Zhang F, Wang L, Liu C et al 2014 *Phys. Lett.* A **378** 1303
[8] Hashemnia K and Pourandi S 2018 *Powder Technol.* **327** 335
[9] Zhang K, Chen T and He L 2017 *Powder Technol.* **321** 173
[10] Ansari I H, Rivas N and Alam M 2018 *Phys. Rev.* E **97** 012911
[11] Zamankhan P 2012 *Chem. Eng. J.* **181** 842
[12] Folli V, Ghofraniha N, Puglisi A et al 2013 *Sci. Rep.* **3** 2251
[13] Jiang Z H, Liang Z J, Wu A C et al 2018 *Physica* A **494** 380
[14] Liu C, Zhang F, Wang L et al 2013 *Powder Technol.* **247** 14
[15] Xie Z A, Wu P, Su T et al 2015 *Powder Technol.* **283** 266
[16] Shinbrot T 2004 *Nature* **429** 352
[17] PachecoV ázquez F and Ruiz-Suárez J C 2010 *Nat. Commun.* **1** 123
[18] van den Wildenberg S, Léopoldès J, Tourin A et al 2017 *EPJ Web Conf.* **140** 03080
[19] Xie Z A, Wu P, Zhang S et al 2012 *Phys. Rev.* E **85** 061302
[20] Fiscina J E, Cáceres M O and Mücklich F 2005 *J. Phys.: Condens. Matter* **17** S1237